GEOPHYSICS, VOL. 38, NO. 3 (JUNE 1973), P. 557-580, 10 FIGS., 7 TABLES

RADIO INTERFEROMETRY DEPTH SOUNDING: PART I—THEORETICAL DISCUSSION†

A. P. ANNAN*

Radio interferometry is a technique for measuring in-situ electrical properties and for detecting subsurface changes in electrical properties of geologic regions with very low electrical conductivity. Ice-covered terrestrial regions and the lunar surface are typical environments where this method can be applied. The field strengths about a transmitting antenna placed on the surface of such an environment exhibit interference maxima and minima which are characteristic of the subsurface electrical properties.

This paper (Part I) examines the theoretical wave nature of the electromagnetic fields about various types of dipole sources placed on the surface of a low-loss dielectric half-space and two-layer earth. Approximate expressions for the fields have been found using both normal mode analysis and the saddle-point method of integration. The solutions yield a number of important results for the radio interferometry depth-sounding method. The half-space solutions show that the interface modifies the directionality of the antenna. In addition, a regular interference pattern is present in the surface fields about the source. The introduction of a subsurface boundary modifies the surface fields with the interference pattern showing a wide range of possible behaviors. These theoretical results provide a basis for interpreting the experimental results described in Part II.

INTRODUCTION

The stimulus for this work was the interest in the measurement of lunar electrical properties in situ and the detection of subsurface layering, if any, by electromagnetic methods. Unlike most regions of the earth's surface, which are conductive largely due to the presence of water, the lunar surface is believed to be very dry and, therefore, to have a very low electrical conductivity (Strangway, 1969; Ward and Dey, 1971). Extensive experimental work on the electrical properties of dry geologic materials by Saint-Amant and Strangway (1970) indicates that these materials are low-loss dielectrics having dielectric constants in the range 3 to 15 and loss tangents considerably less than 1, in the Mhz frequency range. Analysis of the electrical properties of lunar samples by Katsube and Collett (1971) indicates that the lunar surface material has similar electrical properties.

Since electromagnetic methods commonly used in geophysics are designed for conductive earth problems, a method of depth sounding in a dominantly dielectric earth presented a very different problem. One possible method of detecting the presence of a boundary at depth in a dielectric is the radio interferometry technique, first suggested by Stern in 1927 (reported by Evans, 1963) as a method to measure the thickness of glaciers. The only reported application of the technique is the work of El-Said (1956), who attempted to sound the depth of the water table in the Egyptian desert. Although he successfully measured some interference maxima and minima, his method of interpretation of the data is open to question in light of the present work.

† Presented at the 39th Annual SEG International Meeting, September 18, 1969. Manuscript received by the Editor April 6, 1972; revised manuscript received September 22, 1972.

* University of Toronto, Toronto 181, Ontario, Canada.

The radio interferometry technique is conceptually quite simple. The essential features of the method are illustrated in Figure 1. A radio-frequency source placed on the surface of a dielectric earth radiates energy both into the air (or free space) above the earth and downward into the earth. Any subsurface contrast in electrical properties at depth will result in some energy being reflected back to the surface. As a result, there will be interference maxima and minima in the field strengths about the source due to waves traveling different paths. The spatial positions of the maxima and minima are characteristic of the electrical properties of the earth and can be used as a method of inferring the earth's electrical properties at depth.

The problem chosen for study in the theoretical work was that of the wave nature of the fields about various point-dipole sources placed on the surface of a two-layer earth. The mathematical solution to this type of boundary-value problem is found in numerous references. The general problem of electromagnetic waves in stratified media is extensively covered by Wait (1970), Brekhovskikh (1960), Budden (1961), Norton (1937), and Ott (1941, 1943). Although the solu-

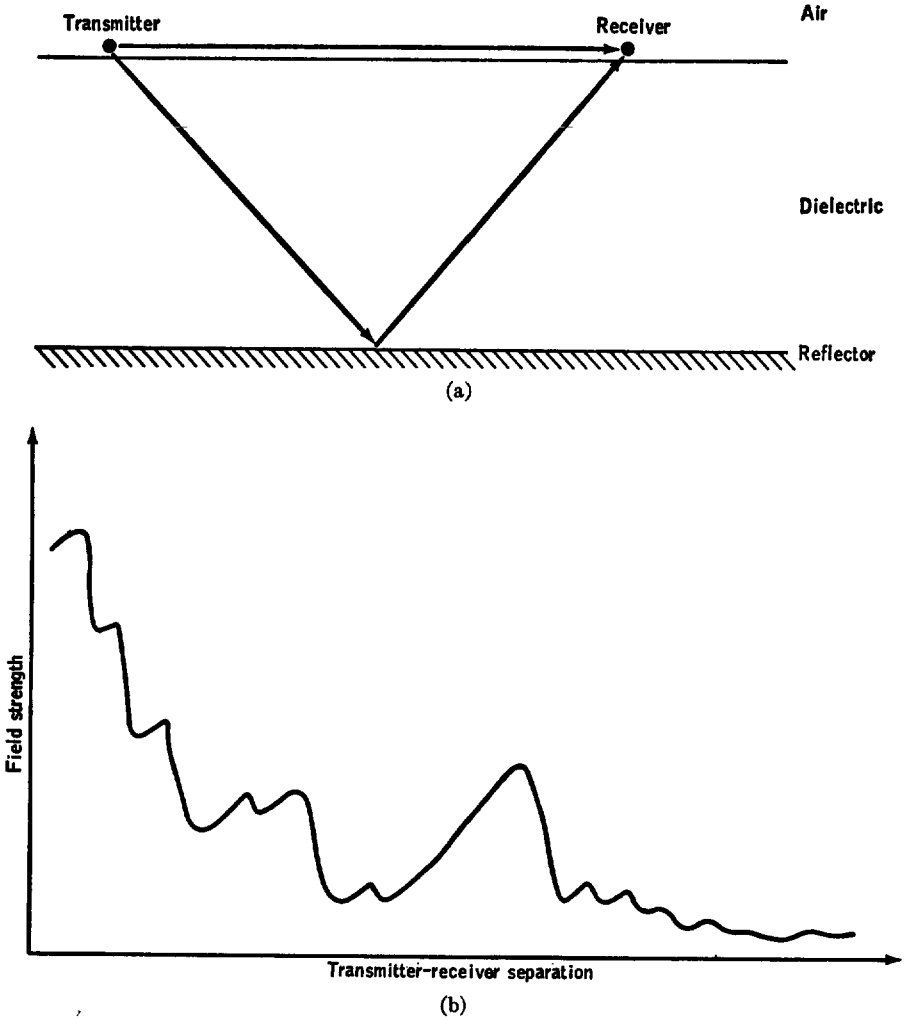

FIG. 1. (a) Transmitter-receiver configuration for radio interferometry, showing a direct wave and a reflected wave. (b) Schematic sketch of typical field-strength maxima and minima as the transmitter-receiver separation increases.

tion to the boundary-value problem can be found analytically, the integral expressions for fields cannot be evaluated exactly. In the radiation zone, approximate solutions to the integrals can be obtained by use of the theory of complex variables and special methods of contour integration. The preceding references, plus numerous others, discuss these techniques in detail. Since much of the detailed work in the mathematical development of these solutions is contained in the above references, the discussion of the solutions that follow will be primarily aimed at the radio interferometry application rather than the mathematical manipulations required to obtain them.

THEORETICAL BOUNDARY-VALUE PROBLEM

Although the various solutions of the boundary-value problem for horizontal and vertical electric and magnetic dipole sources over a two-layer earth appear in the literature, a complete and consistent tabulation of the solutions does not. Therefore, the boundary-value problem is outlined here, and a unified notation is used to express the solutions. This consistent notation is of considerable help in later discussions of the solutions.

The geometry and coordinate systems used in the boundary-value problem are shown in Figure 2. A point-dipole source is located at a height h on the z-axis above a two-layer earth, where the earth's surface is in the x–y-plane at $z=0$, and the subsurface boundary is at $z=-d$. The region $z\geq 0$ is taken as air or free space. The region $-d\leq z<0$ is a low-loss dielectric slab, and the region $z<-d$ is a half-space of arbitrary electrical properties. These regions are denoted 0, 1, and 2, respectively. K_i and M_i are the complex dielectric constant and relative permeability of each region, respectively. For consideration of vertical dipole sources, the dipole moments are taken aligned with the z-axis; for the horizontal dipole sources, the dipole moments are taken aligned parallel to the x-axis.

The solutions are most conveniently written and discussed using the electric and magnetic Hertz vector potential notation. On the assumption of a time dependence $e^{-i\omega t}$ and linear constitutive equations in Maxwell's equations, one obtains the following expressions for the electric and magnetic fields in terms of the Hertz vectors. For electric dipole sources, the electric Hertz vector satisfies the Helmholtz equation,

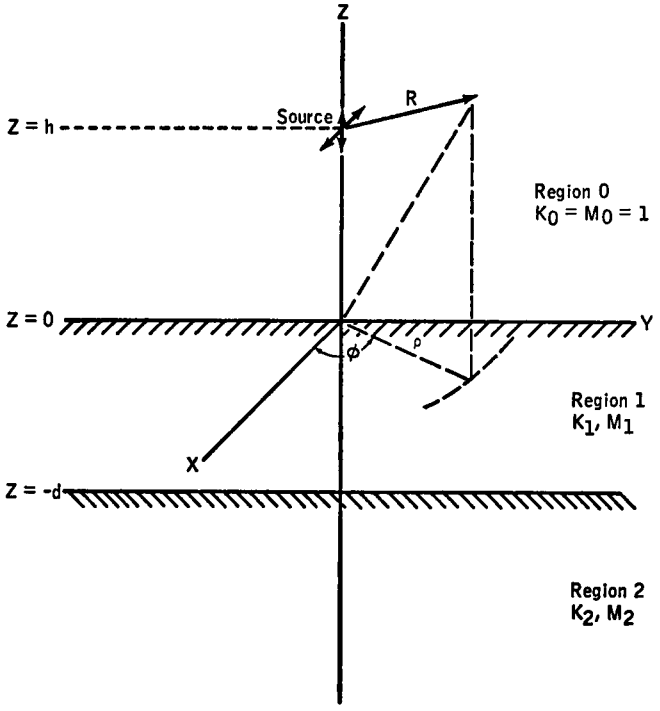

FIG. 2. Geometry of the boundary-value problem for a two-layer earth, showing notation used.

$$\nabla^2\mathbf{\Pi} + k^2\mathbf{\Pi} = -\frac{\mathbf{P}}{K\epsilon_0}, \tag{1}$$

with the electric and magnetic fields defined by

$$\mathbf{E} = k^2\mathbf{\Pi} + \nabla\nabla\cdot\mathbf{\Pi}, \tag{2}$$

and

$$\mathbf{H} = -i\omega K\epsilon_0\nabla\times\mathbf{\Pi} \tag{3}$$

where k is the propagation constant. $\omega\sqrt{KM\epsilon_0\mu_0}$ and ϵ_0, μ_0 denote the permittivity and permeability of free space throughout. $\mathbf{P}$ is the electric dipole moment density distribution. Similarly, for magnetic dipole sources, the results for the magnetic Hertz vector are

$$\nabla^2\mathbf{\Pi} + k^2\mathbf{\Pi} = -\mathbf{M}, \tag{4}$$

and

$$\mathbf{H} = k^2\mathbf{\Pi} + \nabla\nabla\cdot\mathbf{\Pi}, \tag{5}$$

$$\mathbf{E} = i\omega M\mu_0\nabla\times\mathbf{\Pi}, \tag{6}$$

where $\mathbf{M}$ is the magnetic dipole moment density distribution.

The dipole sources are taken as "unit" point dipole sources located in the region $z\geq 0$. The electric dipole moment density distribution is

$$\mathbf{P} = 4\pi\epsilon_0\delta(R)\mathbf{e}_j, \tag{7}$$

where $\mathbf{e}_j$ is a unit vector in the z-direction for a vertical electric dipole source and in the x-direction for the horizontal dipole source. $\delta(R)$ is the three-dimensional delta function, and $R=[x^2+y^2+(z-h)^2]^{1/2}$. Similarly for the magnetic dipole sources,

$$\mathbf{M} = 4\pi\delta(R)\mathbf{e}_j. \tag{8}$$

In the following discussions, no distinction between the electric and magnetic Hertz vectors is made. When we refer to electric dipole sources, the electric Hertz vector is implied; for magnetic dipole sources, the magnetic Hertz vector is implied. In addition, the free-space wavelength is taken as the scaling parameter for all length measurements. In other words, a distance, denoted ρ, is in free-space wavelengths, and the true length is $W\rho$, where W is the free-space wavelength:

$$W = \frac{2\pi}{\omega(\epsilon_0\mu_0)^{1/2}}. \tag{9}$$

This choice of scaling parameter makes all the following integral solutions dimensionless.

As shown by Sommerfeld (1909) for a half-space earth, and extended to a multilayered earth by Wait (1970), the Hertz vectors for the vertical dipole sources have only a z-component, while for the horizontal dipole sources, the Hertz vectors have both x- and z-components. The vertical dipole sources have solutions of the form

$$\Pi_Z^0 = \frac{e^{ik_0R}}{R} + \frac{1}{2W}\int_{-\infty}^{\infty}\frac{\lambda}{P_0}a_0(\lambda)e^{-P_0(Z+h)}H_0^1(\lambda\rho)d\lambda, \tag{10}$$

$$\Pi_Z^1 = \frac{1}{2W}\int_{-\infty}^{\infty}\frac{\lambda}{P_0}\left[a_1(\lambda)e^{P_1Z} + a_2(\lambda)e^{-P_1Z}\right]\cdot e^{-P_0h}H_0^1(\lambda\rho)d\lambda, \tag{11}$$

and

$$\Pi_Z^2 = \frac{1}{2W}\int_{-\infty}^{\infty}\frac{\lambda}{P_0}a_3(\lambda)\cdot e^{P_2Z+(P_2-P_1)d-P_0h}H_0^1(\lambda\rho)d\lambda. \tag{12}$$

λ is the separation constant of the differential equation, and $p_j=(\lambda^2-k_j^2)^{1/2}$, with the sign of the root being chosen such that the solution satisfies the radiation condition. In the above form, after scaling by W, λ is a dimensionless parameter, and $k_j=2\pi(K_jM_j)^{1/2}$ is the relative propagation constant of each region. The $a_j(\lambda)$ are unknown functions of λ which are found by satisfying the boundary conditions that tangential $\mathbf{E}$ and $\mathbf{H}$ be continuous at $z=0$ and $z=-d$.

For horizontal dipole sources, the solutions for the Hertz vector take the form

$$\Pi_x^0 = \frac{e^{ik_0R}}{WR} + \frac{1}{2W}\int_{-\infty}^{\infty}\frac{\lambda}{P_0}b_0(\lambda)e^{-P_0(Z+h)}H_0^1(\lambda\rho)d\lambda, \tag{13}$$

and

$$\Pi_Z^0 = \frac{\cos\phi}{2W}\int_{-\infty}^{\infty}\frac{\lambda^2}{P_0}c_0(\lambda)\cdot e^{-P_0(Z+h)}H_1^1(\lambda\rho)d\lambda \tag{14}$$

for region 0;

$$\Pi_z^1 = \frac{1}{2W}\int_{-\infty}^{\infty} \frac{\lambda}{P_0}\left[b_1(\lambda)e^{P_1 z} + b_2(\lambda)e^{-P_1 z}\right] \cdot e^{-P_0 h}H_0^1(\lambda\rho)d\lambda, \tag{15}$$

and

$$\Pi_z^1 = \frac{\cos\phi}{2W}\int_{-\infty}^{\infty} \frac{\lambda^2}{P_0}\left[c_1(\lambda)e^{P_1 z} + c_2(\lambda)e^{-P_1 z}\right] \cdot e^{-P_0 h}H_1^1(\lambda\rho)d\lambda \tag{16}$$

for region 1; and

$$\Pi_x^2 = \frac{1}{2W}\int_{-\infty}^{\infty} \frac{\lambda}{P_0} b_3(\lambda) \cdot e^{P_2 z+(P_2-P_1)d-P_0 h}H_0^1(\lambda\rho)d\lambda, \tag{17}$$

and

$$\Pi_z^2 = \frac{\cos\phi}{2W}\int_{-\infty}^{\infty} \frac{\lambda^2}{P_0} c_3(\lambda) \cdot e^{P_2 z+(P_2-P_1)d-P_0 h}H_1^1(\lambda\rho)d\lambda \tag{18}$$

for region 2.

The parameters λ and P_j are the same as for the vertical dipole solutions, and the coefficients $b_j(\lambda)$ and $c_j(\lambda)$ are found by satisfying the condition that tangential **E** and **H** be continuous at the boundaries.

The boundary conditions for the Hertz vectors and the resulting expressions for $a_j(\lambda)$, $b_j(\lambda)$, and $c_j(\lambda)$ are tabulated in Appendix A. The expressions for $a_j(\lambda)$, $b_j(\lambda)$, and $c_j(\lambda)$ are written in terms of the *TE* and *TM* Fresnel plane-wave reflection and transmission coefficients. Using this notation, the similarity of all the solutions is clearly emphasized and makes general discussion of the solutions possible rather than dealing with each source separately.

In discussing the approximate evaluation of the above integral expressions, extensive use is made of the plane-wave spectrum concept, since the wave nature of the problem is most clearly understood using this approach. A brief outline of the plane-wave spectrum notation used and approximate evaluation of integrals by the saddle-point method is given in Appendix B.

For radio interferometry applications, the fields at the earth's surface for the source placed at the earth's surface are of primary interest; this corresponds to setting both z and h equal to 0 in the preceding expressions for the Hertz vectors. In the following discussions, h is always set equal to 0, and, in most instances, z is assumed to be close to 0. The solutions are discussed in two parts; the half-space solutions and the two-layer earth solutions. The half-space solutions for the Hertz vectors are obtained by setting $K_1 = K_2$ and $M_1 = M_2$ in expressions (10) through (18). The half-space solution is of considerable interest since the fields about the source show interference maxima and minima without a subsurface reflector present. It also provides a base level for detection of reflections from depth.

APPROXIMATE SOLUTIONS

Half-space earth

The solution of the half-space problem is treated by numerous authors, and the wave nature of the fields is well defined. In the following discussions, the results of Ott (1941) and Brekhovskikh (1960) are followed quite closely, and detailed discussions of various aspects of the solutions can be found in these references. The wave nature of the fields about the source is illustrated in Figure 3. The wavefronts denoted *A* and *B* are spherical waves in the air and earth regions; wave *C* in the air is an inhomogeneous wave, and wave *D* in the earth has numerous names, the most common being head, flank, or lateral wave. Waves *C* and *D* exist only in a limited spatial region, which is defined as those points whose position vectors make an angle greater than α^c with the z-axis. The angle α^c is related to the critical angle of the boundary and is defined in Appendix B.

All the dipole sources exhibit the same wave nature. To demonstrate how the waves are derived from the integral expressions, the vertical magnetic dipole source is used for illustration. In the air, the Hertz vector is given by

$$\Pi_z^0 = \frac{e^{ik_0 R}}{WR} + \frac{ik_0}{2W}\int_c \sin\theta_0 R_{01}(\theta_0) \cdot e^{ik_0 z\cos\theta_0}H_0^1(k_0\rho\sin\theta_0)d\theta_0, \tag{19}$$

and in the earth by

$$\Pi_z^1 = \frac{ik_1}{2W}\int_c \sin\theta_1 T_{10}(\theta_1) \cdot e^{-ik_1 z\cos\theta_1}H_0^1(k_1\rho\sin\theta_1)d\theta_1. \tag{20}$$

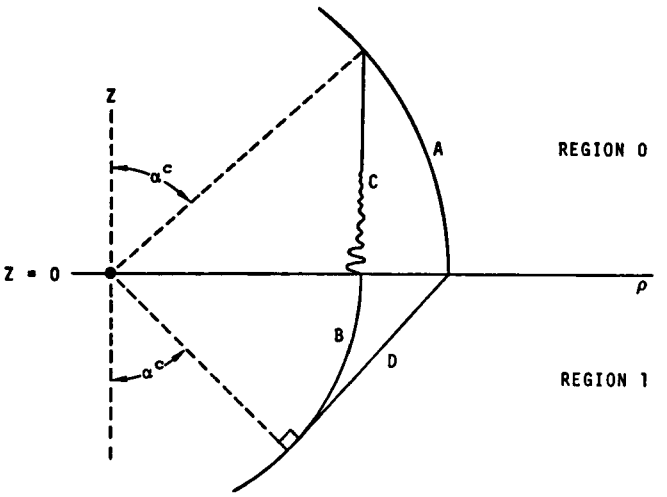

FIG. 3. Wavefronts about a dipole source on the surface of a half-space earth. *A* and *B* are spherical waves in the air and earth, respectively, wave *C* is an inhomogeneous wave in air, and *D* is the head wave in the earth.

With the aid of the Hankel transform identity (Sommerfeld, 1949),

$$\frac{e^{ik_0R}}{WR} = \frac{ik_0}{2W}\int_c \sin\theta_0 \cdot e^{ik_0|Z|\cos\theta_0} H_0^1(k_0\rho\sin\theta_0)\,d\theta_0, \tag{21}$$

and the relation $R_{ij}=T_{ij}-1$ for the Fresnel coefficients, equation (19) becomes

$$\Pi_Z^0 = \frac{ik_0}{2W}\int_c \sin\theta_0 T_{01}(\theta_0) \cdot e^{ik_0|Z|\cos\theta_0} H_0^1(k_0\rho\sin\theta_0)\,d\theta_0. \tag{22}$$

Using the saddle-point method as discussed in Appendix B, the approximate solutions of the integral expressions (20) and (22) are

$$\Pi_Z^0 = \frac{e^{ik_0R}}{WR}\left\{T_{01}(\alpha) - \frac{i}{2k_0R}\left(T_{01}''(\alpha) + \cot\alpha T_{01}'(\alpha)\right)\right\}, \tag{23}$$

and

$$\Pi_Z^1 = \frac{e^{ik_1R}}{WR}\left\{T_{10}(\alpha) - \frac{i}{2k_1R}\left[T_{10}''(\alpha) + \cot\alpha T_{10}'(\alpha)\right]\right\}, \tag{24}$$

where $R=(\rho^2+Z^2)^{1/2}$, and $\alpha=\tan^{-1}\rho/|Z|$. Expressions (23) and (24) correspond to the spherical waves *A* and *B* in Figure 3. The bracketed terms on the right may be interpreted as the modification to the directionality of the source due to the presence of the boundary.

The waves *C* and *D* are generated by crossing the branch points of T_{01} and T_{10} to obtain the saddle-point solutions (23) and (24) for angles $\alpha>\alpha^c$. As outlined in Appendix *B*, the contribution of the branch point can be approximately evaluated by the method of steepest descent as long as α is not close to the branch point. For $\alpha>\alpha^c$ the expressions

$$I_B^0 = \frac{2ik_1\eta_{01}(1-\cot\alpha\tan\theta_{01}^c)^{-3/2}\, e^{ik_1\rho-(k_1^2-k_0^2)^{\frac{1}{2}}Z}}{(k_1^2-k_0^2)W\rho^2}, \tag{25}$$

and

$$I_B^1 = \frac{2ik_0\eta_{10}(1 - \cot\alpha \tan\theta_{10}^c)^{-3/2} e^{ik_0\rho - i(k_1^2 - k_0^2)^{\frac{1}{2}}z}}{(k_1^2 - k_0^2)W\rho^2} \tag{26}$$

must be added to (23) and (24) in order that the solutions be correct. Expression (25) is readily identified as the inhomogeneous wave C, and (26) corresponds to the lateral wave D.

The asymptotic solutions have the form of the geometrical optics solution plus second-order correction terms. For a perfectly dielectric earth, expressions (24) and (26) become infinite as α approaches α^c. The singular behavior arises from the second-order terms which depend on the derivatives of $T_{10}(\theta_1)$. The first-order term which is the geometrical optics solution remains bounded. In this particular case, the angle α^c is the critical angle of $T_{10}(\theta_1)$. As a result, the saddle point and branch point coincide at $\alpha=\alpha^c$, and the approximate methods used to evaluate the integrals are no longer valid. The conical surface about the z-axis, defined by $\alpha=\alpha^c$, is the region where the lateral and spherical waves merge together. In this region the two waves cannot be considered separately; the combined effect of the saddle point and branch point must be evaluated. Detailed analysis of this region for integrals similar to expression (20) is given by Brekhovskikh (1960), who obtains an asymptotic solution with the geometrical optics solution, as the leading term plus a connection term which falls off as $(k_1R)^{-5/4}$ instead of $(k_1R)^{-2}$. This result indicates that the geometrical optics solution still describes the fields adequately for $\alpha \simeq \alpha^c$ when $(k_1R)^{-1/4} \ll 1$. The correction terms given in (24) and (26), however, are not valid when α is close to α^c.

The fields at the earth's surface are of primary interest and are obtained by setting $z=0$ and $\alpha=\pi/2$ in (23), (24), (25), and (26). The solutions given are valid for this region provided the contrast in material properties is not extremely large. In the case of large contrasts, as occur in conductive earth problems, the transmission and reflection coefficients have a pole near $\theta_0=\pi/2$. The pole is located at $\theta_0=\pi-\theta_B$, where θ_B is the Brewster angle. The role of this pole in radio wave propagation over a conductive earth has been the subject of a tremendous amount of discussion since Sommerfeld (1909, 1949) equated the contribution of this pole to the Zenneck surface wave. Numerous people (Norton, 1937; Ott, 1943; Van der Waerden, 1951; Brekhovskikh, 1960; and Wait, 1970) have considered the problem since then using the modified saddle-point technique to evaluate the integrals for $\alpha \simeq \pi/2$. While a true surface wave is not excited, the pole enhances the fields near the source in such a manner that they fall off approximately as $(kR)^{-1}$. At large distances from the source, the fields are those determined by the normal saddle-point method which have a $(kR)^{-2}$ fall off. The transition between the ranges is determined by the proximity of θ_B to $\pi/2$. In the radio interferometry application, the earth properties of interest are those of a low-loss dielectric which is assumed to have only moderate contrasts with the free-space properties. The pole in this case is well away from $\pi/2$ and does not affect the preceding solutions.

In the particular situation of an earth where $M_0=M_1$, the Hertz vector for a vertical magnetic dipole can be evaluated exactly for $z=h=0$. The result is

$$\Pi_Z^0=\Pi_Z^1=\frac{2}{(k_1^2-k_0^2)W\rho^2}\left[e^{ik_0\rho}\left(ik_0-\frac{1}{\rho}\right) - e^{ik_1\rho}\left(ik_1-\frac{1}{\rho}\right)\right], \tag{27}$$

as shown by Wait (1951). This provides a check on the approximate solution. The approximate solution, obtained by adding (23) and (25) or (24) and (26) for $\alpha=\pi/2$, is

$$\Pi_Z^0=\Pi_Z^1=\frac{2i}{(k_1^2-k_0^2)W\rho^2}\left[k_0e^{ik_0\rho}-k_1e^{ik_1\rho}\right], \tag{28}$$

which is the same as (27) if third-order terms are neglected.

The integral expressions for the Hertz vectors for the other dipole sources can be treated in the same manner as for the vertical magnetic dipole. For $z \simeq 0$, in the air, they have the form

$$(-ik_0\cos\phi\sin\alpha)^n\frac{e^{ik_0R}}{WR}\left[G_1(\alpha) + \frac{G_2(\alpha)}{2k_0R}\right] + (\cos\phi)^n(1 - \cot\alpha\tan\theta_{10}^c)^{-3/2} \tag{29}$$

$$\cdot G_3(\alpha)\,\frac{e^{ik_1\rho-(k_1^2-k_0^2)^{\frac{1}{2}}z}}{W\rho^2}.$$

The $G_i(\alpha)$ for the various sources are tabulated in Table 1. The electric and magnetic fields can be obtained by differentiation of the preceding solutions; the particular form of the integrals encountered permits interchange of the integration and differentiation steps.

The half-space solutions demonstrated that interference patterns will be observed in the field strengths even when there is no subsurface reflector. This is readily seen from equation (28). The fields at the earth's surface are composed of two propagating components with one having the phase velocity of the air, and the other the velocity of the earth. Another important feature of the half-space solutions is that the fields near the boundary fall off as the inverse square of the radial distance from the source at distances greater than two or three wavelengths from the source.

A convenient method of interpreting the solutions is to equate the radiation pattern of the source on the boundary to the first-order term in the preceding solutions. This technique demonstrates how the boundary modifies the directionality of the source. The radiation pattern is sharply peaked in the direction of the critical angle into the earth. A sketch of the radiation pattern for a vertical dipole source is shown in Figure 4. This directionality of the source is important when reflections from a subsurface boundary are considered.

Two-layer earth

The analysis of the integral expressions for the two-layer earth problem is carried out in two different ways. The depth of the subsurface boundary and the electromagnetic losses of the first layer determine which approach is more useful. The primary method of analysis is to treat the first layer of the earth as a leaky waveguide and use normal mode analysis. In certain cases the mode analysis is cumbersome, and these cases

Table 1. Coefficients $G_i(\alpha)$ for half-space earth solutions for various dipole sources.

Source	Hertz Vector	n	G_1	G_2	G_3
Vertical Magnetic Dipole	Magnetic Π_Z^0	0	$T_{01}(\alpha)$	$-i(G_1''(\alpha)+G_1'(\alpha)\cot\alpha)$	$-\dfrac{2ik_1\eta_{01}}{k_1^2-k_0^2}$
Vertical Electric Dipole	Electric Π_Z^0	0	$S_{01}(\alpha)$	$-i(G_1''(\alpha)+G_1'(\alpha)\cot\alpha)$	$-\dfrac{2ik_1\xi_{01}}{k_1^2-k_0^2}$
Horizontal Magnetic Dipole	Magnetic Π_X^0	0	$S_{01}(\alpha)$	$-i(G_1''(\alpha)+G_1'(\alpha)\cot\alpha)$	$-\dfrac{2ik_1\xi_{01}}{k_1^2-k_0^2}$
	Magnetic Π_Z^0	1	$\dfrac{(\gamma_{01}-1)T_{01}(\alpha)S_{01}(\alpha)}{2P_0(\alpha)}$	$-i(G_1''(\alpha)+3G_1'(\alpha)\cot\alpha-2G_1(\alpha))$	$\dfrac{2ik_0^2(\xi_{10}+\eta_{10})}{k_1^2(k_0^2-k_1^2)^{1/2}}$
Horizontal Electric Dipole	Electric Π_X^0	0	$T_{01}(\alpha)$	$-i(G_1''(\alpha)+G_1'(\alpha)\cot\alpha)$	$-\dfrac{2ik_1\eta_{01}}{k_1^2-k_0^2}$
	Electric Π_Z^0	1	$\dfrac{(\gamma_{01}-1)T_{01}(\alpha)S_{01}(\alpha)}{2P_0(\alpha)}$	$-i(G_1''(\alpha)+3G_1'(\alpha)\cot\alpha-2G_1(\alpha))$	$\dfrac{2ik_0^2(\eta_{10}+\xi_{10})}{k_1^2(k_0^2-k_1^2)^{1/2}}$

Definition: $G_1'(\alpha)=\left.\dfrac{dG_1(\theta_0)}{d\theta_0}\right|_{\theta_0=\alpha}$ $\qquad$ $G_1''=\left.\dfrac{d^2G_1(\theta_0)}{d\theta_0^2}\right|_{\theta_0=\alpha}$

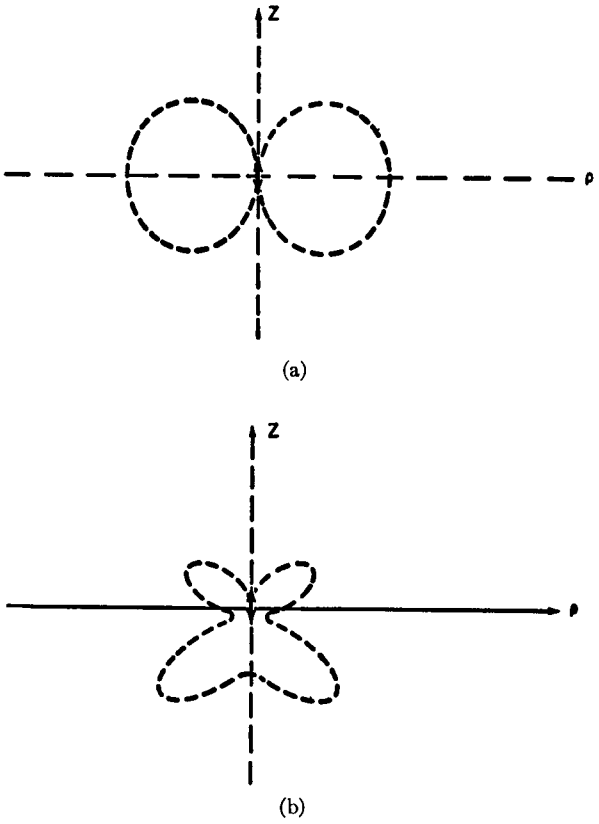

FIG. 4. Sketch showing how a dielectric boundary modifies the directionality of a vertical dipole source placed on the boundary. (a) No boundary present. (b) Boundary at $Z=0$.

yield more useful results when the integrals are solved approximately using the saddle-point method of integration.

The various dipole sources may all be treated in the same manner. For the purpose of illustrating the method of analysis, the horizontal electric dipole source solutions are used as an example. The x- and z-components of the electric Hertz vector in the air for this source are given by equations (13) and (14) where the coefficients b_0 and c_0 are listed in Table A-2.

For normal mode analysis, equation (13) is rewritten using the integral identity [equation (21)]. The components of the Hertz vector are given by

$$\Pi_x^0 = \frac{ik_1}{2W}\int_c \sin\theta_1 m_{10}(\theta_1)[1 + b_0(\theta_1)] \cdot e^{ik_{0Z}\cos\theta_0} H_0^1(k_{1\rho}\sin\theta_1)d\theta_1, \quad (30)$$

and

$$\Pi_z^0 = \cos\phi\,\frac{ik_1^2}{2W}\int_c \sin^2\theta_1 m_{10}(\theta_1)c_0(\theta_1) \cdot e^{ik_0\cos\theta_0 Z} H_1^1(k_{1\rho}\sin\theta_1)d\theta_1, \quad (31)$$

where the integration variable is θ_1, as defined in Appendix B. The singularities of the coefficients b_0 and c_0 determine the nature of the solutions to equations (30) and (31).

The expressions

$$m_{10}(1 + b_0) = \frac{\eta_{10}T_{10}(1 + R_{12}\beta)}{1 - R_{10}R_{12}\beta}, \quad (32)$$

and

$$m_{10}c_0 = \frac{1}{2\rho_0} \cdot \left[\frac{(\gamma_{01}-1)\eta_{10}T_{10}(1+R_{12}\beta)S_{01}(1+X_{12}\beta)}{(1-X_{10}X_{12}\beta)(1-R_{10}R_{12}\beta)}\right.$$

$$-\frac{(\gamma_{21}-1)\xi_{10}S_{10}S_{12}\gamma_{01}T_{01}\gamma_{12}T_{12}\beta}{(1-X_{10}X_{12}\beta)(1-R_{10}R_{12}\beta)}\Bigg] \quad (33)$$

have branch points at the two critical angles of the two boundaries in question. In addition, equation (32) has an infinite set of simple poles, and (33) has a doubly infinite set of poles on each Riemann surface. These poles are determined by the normal mode equations,

$$1 - R_{10}R_{12}\beta = 0, \quad (34)$$

and

$$1 - X_{10}X_{12}\beta = 0. \quad (35)$$

Equations (34) and (35) are the TE and TM normal mode equations, respectively. Both are transcendental equations with infinite sets of roots. The relation between the normal modes and multiple reflections is readily obtained by expanding the denominators of equations (32) and (33) into infinite geometric series. For example,

$$(1 - R_{10}R_{12}\beta) = \sum_{n=0}^{\infty} (R_{10}R_{12}\beta)^n. \quad (36)$$

The positions of the poles and branch points in the complex plane determine the wave nature of the solutions to equations (30) and (31). The normal mode solutions are obtained by deforming the contour of integration C to C', as schematically illustrated in Figure 5. The integral from $-(\pi/2)+i\infty$ to $\pi/2+i\infty$, and from $\pi/2+i\infty$ to $\pi/2-i\infty$ is identically zero. Along the first part of C' the integral is zero since the integrand is zero. Along the second part of the contour C' the integral is zero due to the asymmetry of the integrand about $\theta_1=\pi/2$. This result is common in mode analysis and has a wide range of applications as discussed in detail by Brekhovskikh (1960). The integral along C is equal to the residues of the poles crossed in deforming the contour to C', plus the integrals along contours C_1 and C_2 which run from $+i\infty$ around the branch points and back to $+i\infty$. The components of the Hertz vector are given by

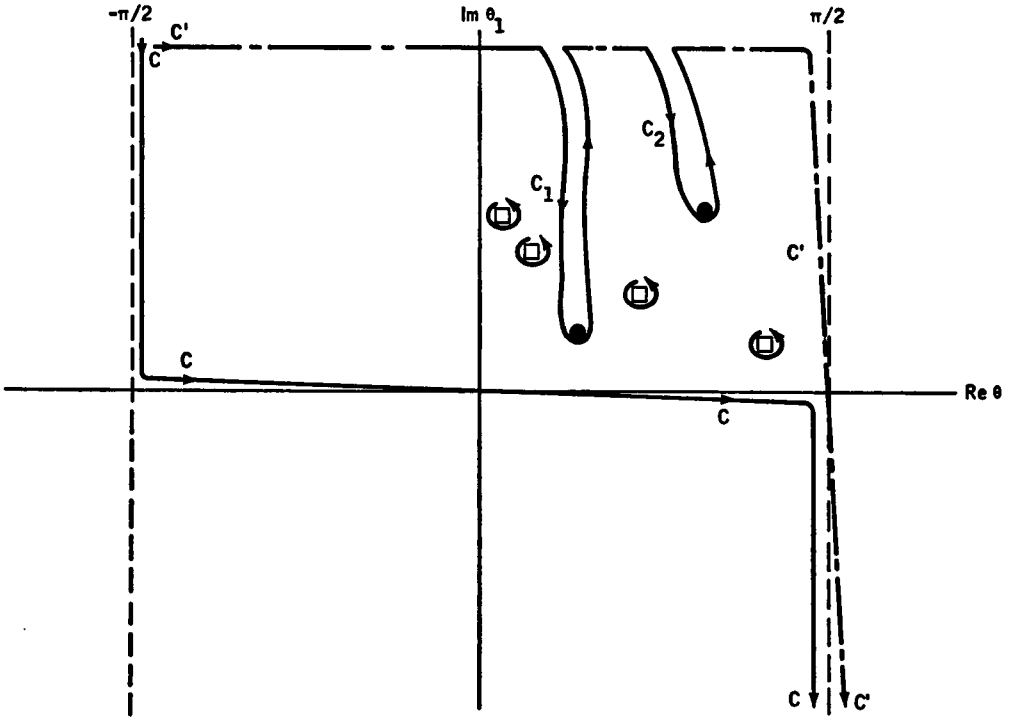

FIG. 5. Complex θ_1-plane showing how integration contour C is modified to C' in order to obtain normal mode solutions. Branch points denoted by solid circles and the poles by squares.

Table 2. Residues of poles for normal mode analysis for horizontal electric dipole.

Π_X^0 *TE* Mode Residue	$\dfrac{ik_1 \sin\theta_1^P \eta_{10} T_{10}(\theta_1^P)[1 + R_{12}(\theta_1^P)\beta(\theta_1^P)] e^{ik_0(1-\gamma_{10}\sin^2\theta_1^P)^{1/2}Z}}{2W\left(i2k_1 d\cos\theta_1^P - \dfrac{\partial \ln R_{10}(\theta_1)R_{12}(\theta_1)}{\partial\theta_1}\right)\Big\vert_{\theta_1=\theta_1^P}} H_0^1(k_1\rho\sin\theta_1^P)$
Π_Z^0 *TE* Mode Residue	$\dfrac{\cos\phi ik_1^2 \sin^2\theta_1^P t(\theta_1^P) e^{ik_0(1-\gamma_{10}\sin^2\theta_1^P)^{1/2}Z}}{2W[1 - X_{10}(\theta_1^P)X_{12}(\theta_1^P)\beta(\theta_1^P)]\left(i2k_1 d\cos\theta_1^P - \dfrac{\partial \ln R_{10}(\theta_1)R_{12}(\theta_1)}{\partial\theta_1}\right)\Big\vert_{\theta_1=\theta_1^P}} H_1^1(k_1\rho\sin\theta_1^P)$
Π_Z^0 *TM* Mode Residue	$\dfrac{\cos\phi ik_1^2 \sin^2\theta_1^P t(\theta_1^P) e^{ik_0(1-\gamma_{10}\sin^2\theta_1^P)^{1/2}Z}}{2W[1 - R_{10}(\theta_1^P)R_{12}(\theta_1^P)\beta(\theta_1^P)]\left(i2k_1 d\cos\theta_1^P - \dfrac{\partial \ln X_{10}(\theta_1)X_{12}(\theta_1)}{\partial\theta_1}\right)\Big\vert_{\theta_1=\theta_1^P}} H_1^1(k_1\rho\sin\theta_1^P)$

where $t(\theta_1^P) = \dfrac{(\gamma_{01}-1)}{2P_0(\theta_1^P)}[\eta_{10}T_{10}(\theta_1^P)[1 + R_{12}(\theta_1^P)\beta(\theta_1^P)]S_{01}(1 + X_{12}(\theta_1^P)\beta(\theta_1^P))]$

$$- \frac{(\gamma_{21}-1)}{2P_0(\theta_1^P)}[\xi_{10}S_{10}(\theta_1^P)S_{12}(\theta_1^P)\gamma_{01}T_{01}(\theta_1^P)\gamma_{12}T_{12}(\theta_1^P)\beta(\theta_1^P)]$$

$$\Pi_x^0 = 2\pi i \sum (TE \text{ pole residues}) + I_1 + I_2, \tag{37}$$

and

$$\Pi_Z^0 = 2\pi i \sum (TE \text{ pole residues}) + 2\pi i \sum (TM \text{ pole residues}) + I_3 + I_4, \tag{38}$$

where

$$I_1 = \frac{ik_1}{2W}\int_{c_1} \sin\theta_1 m_{10}(\theta_1)[1 + b_0(\theta_1)] \cdot e^{ik_0 Z\cos\theta_0} H_0^1(k_1\rho\sin\theta_1)d\theta_1, \tag{39}$$

$$I_2 = \frac{ik_1}{2W}\int_{c_2} \sin\theta_1 m_{10}(\theta_1)[1 + b_0(\theta_1)] \cdot e^{ik_0 Z\cos\theta_0} H_0^1(k_1\rho\sin\theta_1)d\theta_1, \tag{40}$$

$$I_3 = \cos\phi\,\frac{ik_1^2}{2W}\int_{c_1} \sin^2\theta_1 m_{10}(\theta_1)c_0(\theta_1) \cdot e^{ik_0 Z\cos\theta_0} H_1^1(k_1\rho\sin\theta_1)d\theta_1, \tag{41}$$

$$I_4 = \cos\phi\,\frac{ik_1^2}{2W}\int_{c_2} \sin^2\theta_1 m_{10}(\theta_1)c_0(\theta_1) \cdot e^{ik_0 Z\cos\theta_0} H_1^1(k_1\rho\sin\theta_1)d\theta_1. \tag{42}$$

The solutions (37) and (38) are completely general and valid provided a branch point and a pole, or a *TE* and *TM* pole, do not coincide. In the first situation, the pole and branch-point contributions must be considered together rather than separately, as indicated. In the other situation, (38) must include the residue of a second-order pole rather than the residues of two simple poles, as indicated. Since these situations rarely occur, they are not discussed further here.

The expressions for the residues in (37) and (38) are tabulated in Table 2. Approximate solutions to the branch cut integrals may be obtained by steepest-descent integration as discussed in Appendix B. The solutions are the second-order lateral and inhomogeneous waves generated at the boundaries. The approximate solutions are listed in Table 3.

The behavior of the fields at the earth's surface is very dependent on the position of the singular points in the complex θ_1 plane, which points are, in turn, determined by the material properties of the earth and the layer thickness d. The important features of the solutions are the radial dependences and the initial amplitudes of the various terms in the solutions. All the residues contain Hankel functions, which, for radial distances greater than one or two wavelengths, have the form

Table 3. Approximate steepest-descent solutions to branch-cut integrals for normal mode analysis of the horizontal electric dipole.

I_1	$\dfrac{2ik_0\eta_{10}^2(1+R_{12}(\theta_{10}^c)\beta(\theta_{10}^c))^2 e^{ik_0\rho}}{(k_1^2-k_0^2)(1-R_{12}(\theta_{10}^c)\beta(\theta_{10}^c))^2 W\rho^2}$
I_2	$\dfrac{2ik_1^2\eta_{20}T_{10}^2(\theta_{12}^c)(1-\cot\alpha_d\tan\theta_{12}^c)^{-3/2} e^{ik_{2\rho}-2d(k_2^2-k_1^2)^{1/2}-(k_2^2-k_0^2)^{1/2}Z}}{k_2(k_1^2-k_0^2)(1-R_{10}(\theta_{12}^c)\beta(\theta_{12}^c))^2 W\rho^2}$
I_3	$-\dfrac{\cos\phi k_0}{2(k_1^2-k_0^2)^{1/2}}\left[\dfrac{C_1(\theta_{10}^c)e^{ik_0\rho}}{W\rho^2}+\dfrac{(1-\cot\alpha_d\tan\theta_{10}^c)^{-3/2}C_2(\theta_{10}^c)e^{ik_0\rho+i2d(k_1^2-k_0^2)^{1/2}}}{W\rho^2}\right]$
I_4	$-\dfrac{\cos\varphi k_2(1-\cot\alpha_d\tan\theta_{12}^c)^{-3/2}C_3(\theta_{12}^c)\, e^{ik_{2\rho}-(k_2^2-k_1^2)^{1/2}2d-(k_2^2-k_0^2)^{1/2}Z}}{2(k_1^2-k_2^2)^{1/2}W\rho^2}$
$C_1(\theta_{10}^c)$	$\dfrac{4i\gamma_{10}}{k_0}\left[\dfrac{\eta_{01}(1-R_{12}^2\beta^2)(1+X_{12}\beta)^2+\xi_{01}(1-X_{12}^2\beta^2)(1+R_{12}\beta)^2}{(1-X_{12}\beta)^2(1-R_{12}\beta)^2}\right]$
$C_2(\theta_{10}^c)$	$\dfrac{4i\gamma_{10}(1-\gamma_{12})\gamma_{01}S_{12}T_{12}[\eta_{01}(1+X_{12}\beta)(1-R_{12}\beta)+\xi_{01}(1-X_{12}\beta)(1+R_{12}\beta)]}{k_0(1-\gamma_{01})(1-X_{12}\beta)^2(1-R_{12}\beta)^2}$
$C_3(\theta_{12}^c)$	$\dfrac{2i\eta_{10}T_{10}S_{01}\sqrt{\gamma_{21}}\{(\gamma_{01}-1)[\xi_{12}S_{10}(1+T_{01}\beta-R_{10}\beta^2)+\eta_{12}T_{10}(1+S_{01}\beta-X_{10}\beta^2)]-2(1-\gamma_{12})\gamma_{01}\gamma_{12}[\xi_{21}(1+X_{10}\beta)(1-R_{10}\beta)+\eta_{21}(1-X_{10}\beta)(1+R_{10}\beta)]\}}{k_0(1-\gamma_{20})^{1/2}(1-\gamma_{21})^{1/2}(1-X_{10}\beta)^2(1-R_{12}\beta)^2}$
	$\sin\theta_{10}^c=\dfrac{k_0}{k_1}\qquad \sin\theta_{12}^c=\dfrac{k_2}{k_1}\qquad \alpha_d=\tan^{-1}\left\lvert\dfrac{2d}{\rho}\right\rvert$

$$\rho^{-1/2}e^{ik_1\rho\sin\theta_1^p}, \tag{43}$$

where θ_1^p is a pole defined by equations (34) and (35). The branch cut contributions, I_1 and I_3, fall off as ρ^{-2} with no exponential attenuation, while I_2 and I_4 fall off as ρ^{-2} and are exponentially attenuated when the earth is lossy. The amplitudes of the modes are largest for those poles in the vicinity of θ_{10}^c. This effect is related to the modified directionality of the source as discussed for the half-space fields. When the earth has a finite loss all terms in the solution except I_1 and the first term of I_3 have amplitudes which decay exponentially with increasing loss or increasing d.

The positions of the poles in the complex θ_1 plane for three idealized models are illustrated schematically in Figure 6. The earth consists of a perfect dielectric slab over a half-space, which is a perfect conductor in case (a), a perfect dielectric with $K_2>K_1$ in case (b), and a perfect dielectric with $K_2<K_1$ in case (c). In all cases $M_0=M_1=M_2$ is assumed since permeabilities of bulk earth materials vary little from the free-space value. The poles lie on the lines $|R_{10}R_{12}\beta|=1$ and $|X_{10}X_{12}\beta|=1$, with the density of distribution of the poles on these lines controlled by the slab thickness d. For d small, the poles are widely spaced with most of them lying high up the lines near the imaginary θ_1 axis. For increasing d, the poles move down the lines toward $\theta_1=\pi/2$ and are more closely packed. Unattenuated modes occur only when the θ_1^p lie on or close to the real θ_1 axis. In case (a), the pole contours lie on the real axis for $\theta_{10}^c\leq\theta_1\leq\pi/2$; unattenuated modes can be excited when θ_1 exceeds the critical angle of the free-space-earth interface. In case (c), the slab forms a dielectric waveguide when θ_1 is greater than the critical angles of both boundaries. For both (a) and (c), the modes with real θ_1^p less than the largest critical angle are highly damped due to energy leaking out of the slab. In

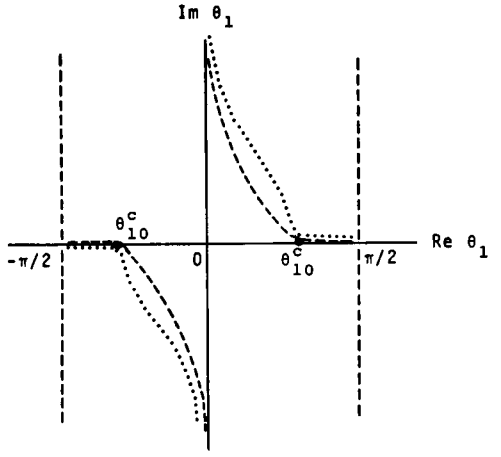

$K_0 = 1$	FREE SPACE
K_2	PERFECT DIELECTRIC
	PERFECT CONDUCTOR

(a)

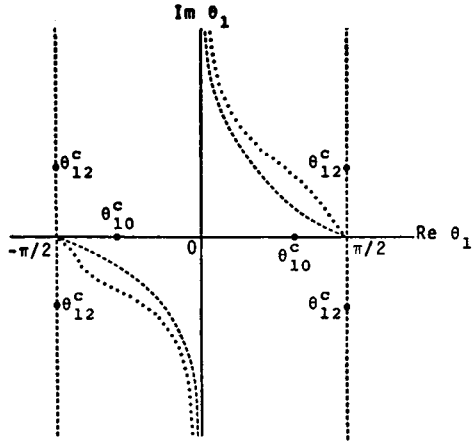

$K_0 = 1$	FREE SPACE
K_1	PERFECT DIELECTRIC
$K_2 > K_1$	PERFECT DIELECTRIC

(b)

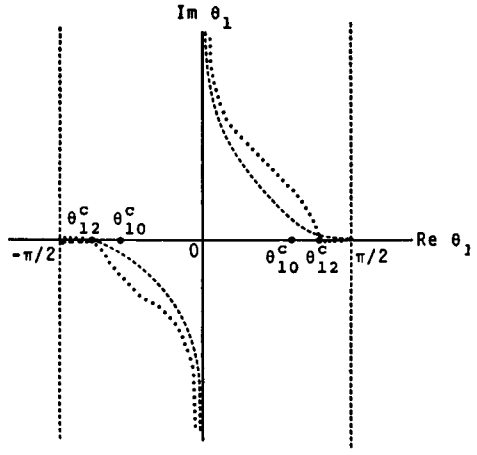

$K_0 = 1$	FREE SPACE
K_1	PERFECT DIELECTRIC
$K_2 < K_1$	PERFECT DIELECTRIC

(c)

FIG. 6. Sketches of complex θ_1-plane showing positions of branch points and pole lines for 3 simple two-layer earth cases; case (a), dielectric slab over a perfect conductor; case (b), dielectric slab over dielectric half-space with $K_2 > K_1$; case (c) dielectric slab over a dielectric half-space with $K_2 < K_1$. The dashed lines are contours where $|R_{10}R_{12}\beta| = 1$; the dotted lines are contours where $|X_{10}X_{12}\beta| = 1$; the branch points are denoted by solid circles.

case (b), no unattenuated mode can exist, since energy is continually flowing out of the slab into the lower half-space. The effect of a finite loss in the slab moves the pole contours up away from the real axis, and all modes have a finite attenuation. These models demonstrate the general position and behavior of the singular points in the complex plane. More detailed studies are given by Wait (1970), Brekhovskikh (1960), and Budden (1961).

The normal mode approach is most useful when the distance from the source is greater than the depth of the boundary d and when the earth has a very low loss. In a lossy dielectric, the complex dielectric constant is $K'(1+i\tan\delta)$, where K' is the real dielectric constant and $\tan\delta$ is the loss tangent; and the attenuation distance in free-space wavelengths for a plane wave is

$$D = \frac{1}{\pi\sqrt{K'}\tan\delta}, \tag{44}$$

when $\tan\delta \ll 1$. When d approaches the attenuation distance, the solutions begin to approach those of a lossy dielectric half-space. An alternate approach to evaluating the fields when the distance from the source is less than d, or when $d \geq D$, is desirable, since the normal mode approach is cumbersome in these cases.

The integrals can be approximately evaluated by the saddle-point method of integration when multiple reflections are not strong. The fields can then be expressed as the half-space solution plus a contribution from the subsurface boundary. By regrouping the coefficients b_0 and c_0 in the form

$$b_0 = R_{01} + b_0^1\beta, \tag{45}$$

$$c_0 = \frac{1}{2}(\gamma_{01} - 1)\frac{S_{01}T_{01}}{P_0} + c_0^1\beta, \tag{46}$$

$$b_0^1 = \frac{T_{01}T_{10}R_{12}}{(1 - R_{10}R_{12}\beta)}, \tag{47}$$

and

The Hertz vector components can then be written as

$$\Pi_x^0 = L_1 + L_2, \tag{49}$$

and

$$\Pi_z^0 = L_3 + L_4, \tag{50}$$

where L_1 and L_3 are the half-space earth solutions discussed earlier, and L_2 and L_4, given by

$$L_2 = \frac{ik_1}{2W}\int_c \sin\theta_1 m_{10} b_0^1(\theta_1) \cdot e^{ik_0 z\cos\theta_0}\beta H_0^1(k_1\rho\sin\theta_1)d\theta_1, \tag{51}$$

and

$$L_4 = \cos\phi\,\frac{ik_1^2}{2W}\int_c \sin^2\theta_1 m_{10} c_0^1(\theta_1) \cdot e^{ik_0 z\cos\theta_0}\beta H_1^1(k_1\rho\sin\theta_1)d\theta_1 \tag{52}$$

describe the effect of the subsurface boundary.

L_2 and L_4 can be approximately evaluated by the saddle-point method, which results in the geometric optics solution. Since z is assumed close to zero throughout, the expression

$$\beta H_n^1(k_1\rho\sin\theta_1) \tag{53}$$

in the integrands may be regrouped using the asymptotic expansion of the Hankel function in the manner discussed in Appendix B. L_2 and L_4 then contain the expression

$$e^{i2k_1 d\cos\theta_1 + ik_1\rho\sin\theta_1} = e^{ik_1 R_d\cos(\theta_1 - \alpha_d)} \tag{54}$$

in the integrand, where $R_d = (\rho^2 + 4d^2)^{1/2}$ and $\alpha_d = \tan^{-1}(\rho/2d)$. In this form α_d is the saddle point of the integrand and is the geometric optics direction of a ray reflected from the subsurface boundary. The saddle-point solutions of L_2 and L_4, outlined in Appendix B, are

$$c_0^1 = \frac{1}{2P_0}\left[\frac{(\gamma_{01} - 1)S_{01}T_{01}[T_{10}R_{12} + S_{10}X_{12} + (S_{01} + T_{01} - S_{21}T_{01})X_{12}R_{12}\beta]}{(1 - R_{10}R_{12}\beta)(1 - X_{10}X_{12}\beta)} - \frac{(\gamma_{21} - 1)\xi_{10}S_{10}S_{12}m_{01}T_{01}\gamma_{12}T_{12}}{(1 - R_{10}R_{12}\beta)(1 - X_{10}X_{12}\beta)}\right]. \tag{48}$$

$$L_2 \approx \frac{e^{ik_1R_d}}{WR_d}\left[P(\alpha_d) - \frac{i}{2k_1R_d}\left(P''(\alpha_d) + P'(\alpha_d)\cot\alpha_d\right)\right], \quad (55)$$

and

$$L_4 = \cos\phi \sin\alpha_d \frac{e^{ik_1R_d}}{WR_d} \cdot\left[Q(\alpha_d) - \frac{i}{2k_1R_d}\left(Q''(\alpha_d) + 3\cot\alpha_d Q'(\alpha_d) - 2Q(\alpha_d)\right)\right], \quad (56)$$

where

$$P = m_{10}(\alpha_d)b_0^1(\alpha_d)e^{ik_0Z(1-\gamma_{10}\sin^2\alpha_d)^{1/2}}, \quad (57)$$

and

$$Q = m_{10}(\alpha_d)c_0^1(\alpha_d)e^{ik_0Z(1-\gamma_{10}\sin^2\alpha_d)^{1/2}}. \quad (58)$$

Expressions (55) and (56) can be interpreted as having replaced the subsurface boundary by an image source at twice the depth. The image source has a radiation pattern which depends on the reflection and transmission coefficients of the boundaries and the layer thickness.

In obtaining the saddle-point solution, the effect of the poles and branch points has been neglected; such neglect is justified when the boundary is deep and the earth has a significant loss. This is illustrated in Figure 7. To obtain the saddle-point contribution, the integration contour C must be deformed into the saddle-point contour Γ. The position of Γ in the complex θ_1 plane is determined by α_d, which, in turn, is determined by the ratio of the radial distance to the depth of the boundary, $\rho/2d$. In order that a given pole or branch point be crossed when C is deformed to Γ, α_d must exceed a certain value which is determined by equation (B-11), which defines the contour Γ. Since $\rho = 2d \tan\alpha_d$, the radial distance from the source at which the singular point is

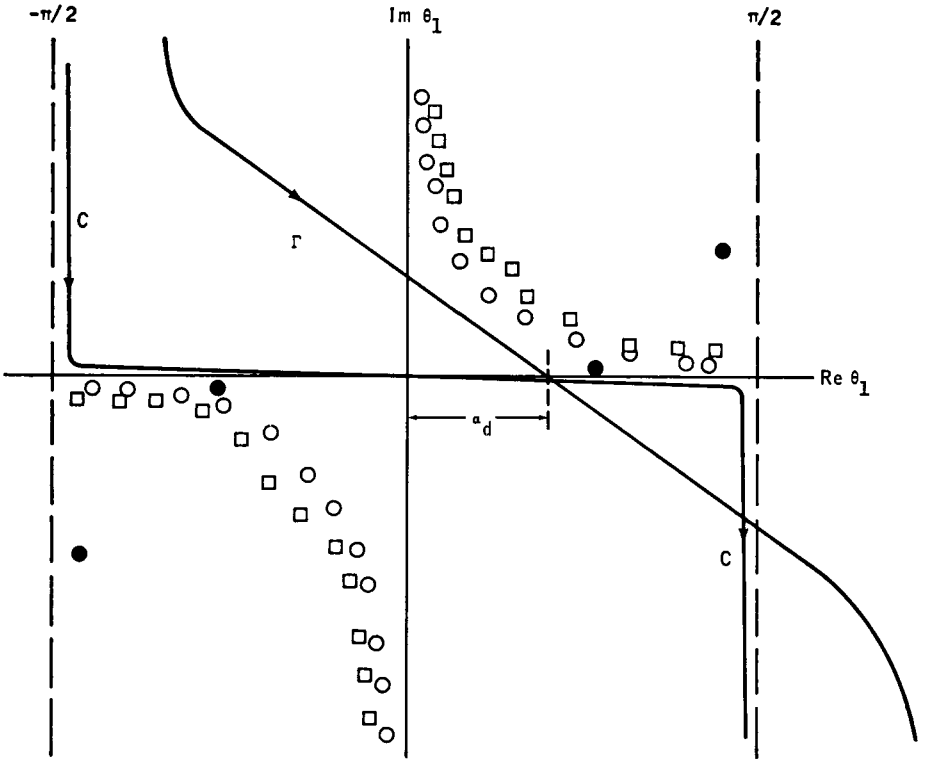

FIG. 7. Complex θ_1-plane showing deformation of contour C to saddle-point contour Γ. Solid circles = branch points, squares = TE poles, and open circles = TM poles.

crossed in obtaining Γ is defined. When the singular point is a pole, the contribution to the integral after crossing the pole is a residue of a form similar to those in Table 2. When the pole is not on the real θ_1 axis, the residue is exponentially attenuated with increasing radial distance. The value of ρ at which the pole must be considered in determining the integral is also defined, and is usually much greater than the attenuation distance of the mode. As a result, the residue of the pole is extremely small and is negligible compared to the saddle-point contribution. For cases when some poles lie on or near the real θ_1 axis, a fixed radial distance from the source must be exceeded before their effect needs to be considered. Beyond this distance, the normal mode approach is more convenient for expressing the solutions.

The branch-point contributions yield inhomogeneous and lateral waves generated at or reflected from the subsurface boundary. As in the case of the poles, a finite distance from the source must be exceeded before these contributions need to be considered. For the earth models where the saddle-point method is useful, these contributions, which are second-order effects, are negligible. When these second-order waves are significant in the determination of the field strengths at the earth's surface, the normal mode approach is the better method for computing the fields.

The two-layer earth solutions cover a wide range of possible responses. The important results are as follows:

1. When the first layer of the earth is very thin and the second layer is a low-loss medium, the first layer is undetectable. The response of the earth is the same as that of a half-space composed of the second layer of the earth.

2. When the first layer of the earth is on the order of one wavelength thick, the surface fields become extremely complex. The fields exhibit a $\rho^{-1/2}$ fall-off out to the attenuation distance of the least attenuated mode which is strongly excited. Beyond this distance, the contribution of the modes becomes negligible and the second-order lateral and inhomogeneous waves, with no radial exponential attenuation, determine the field strengths which then fall off as ρ^{-2}. When modes with low attenuation are excited, they are generally few in number. Since each propagates radially with a different phase velocity, the fields will show a regular periodic beating as the various modes move in- and out-of-phase.

3. When the first layer of the earth is lossy and several wavelengths deep, the geometric optics solution is more useful than the normal mode approach. The expression for the fields is the half-space solution plus a contribution from the reflecting boundary. This is the type of solution used by El-Said (1956). In El-Said's analysis, the waves propagating along the surface were not correctly expressed, and the modification in directionality of the source due to the air-earth interface was not considered. This form of solution is particularly useful for a quick computation of the strength of reflections from subsurface boundaries and of the effect on surface fields of changes in electrical properties.

4. The saddle-point solution is useful for determining the radial distance from the source at which the various contributions of the singularities of the integrand become important. Since the saddle-point contour is positioned in the complex plane by the ratio $\rho/2d$, a ratio $\rho/2d$ can be defined for each singularity. For normal modes, the radial distance defined by this ratio may be interpreted as the distance from the source required for a given mode to develop. For the branch points, this ratio defines the critical distances from the source, where lateral waves and inhomogeneous waves from the subsurface boundary reach the surface.

DISCUSSION

The radio interferometry technique provides a method of determining electrical properties in situ and of detecting subsurface stratification of the electrical properties in environments which are moderately transparent to electromagnetic waves. The theoretical analysis of the two-layer earth problem defines the behavior of the fields at the earth's surface and provides a basis for understanding experimental results reported by Rossiter et al (1973) in Part II. The various solutions derived here are also useful for computing rough estimates of the interference patterns in the fields at the earth's surface, provided the asymptotic

nature of the expressions is given due respect. Examples of these are given in Part II.

The half-space solutions provide a method of determining the electrical properties for a half-space. Any strong departures from the half-space wave nature (i.e., a regular interference pattern and a ρ^{-2} distance dependence) indicate that reflections from depth are important. When the reflections from depth are due to a horizontal boundary in electrical properties, the behavior of the fields varies considerably. For example, when normal modes are excited, the fields fall off as $\rho^{-1/2}$ with regular beating in the field strengths with distance from the source.

The treatment of a two-layer earth with plane boundaries, homogeneous media, and point sources is a considerable simplification of most real environments. These simple models and the approximate solutions obtained do, however, provide insight into the field behavior in the radio interferometry application. Methods to accurately compute field strengths for these models are currently under investigation. The effect of rough and dipping boundaries on the solutions is extremely important. Also, the presence of scattering by inhomogeneities in the earth can drastically alter the fields at the earth's surface. These problems are virtually impossible to treat in a general manner theoretically. Scale model experiments seem to be the most feasible method of studying these problems. This work is presently in progress.

The free-space wavelength provides the most useful unit of length when discussing and plotting radio interferometry data. Scale model construction is based on keeping all dimensions the same on the wavelength scale and having the same loss tangent. In the analysis of field data, plotting distances on a wavelength scale makes comparison of data taken at different frequencies straightforward. If the electrical properties are not frequency dependent, running the experiment using several different frequencies can effectively vary the depth of a subsurface interface from a fraction of a wavelength to many wavelengths.

APPENDIX A: COEFFICIENTS AND PARAMETERS

The coefficients in the integral expressions for the Hertz vectors for the various dipole sources are obtained by satisfying the boundary conditions at $z=0$ and $z=-d$. Without a consistent notation, the coefficients are extremely complicated expressions, which lose the symmetry of equations (1) through (6) and are difficult to interpret physically. In this section, the solutions for the coefficients are tabulated, and the notation used throughout the body of the text is defined.

In Table A-1, the boundary conditions for the Hertz vectors are listed. In Table A-2, the expressions for the $a_j(\lambda)$, $b_j(\lambda)$, and $c_j(\lambda)$ are listed for each dipole source. Examination of these solutions shows the symmetry between the electric and magnetic dipole sources. Interchanging the roles of K_i and M_i, one can readily obtain the solution for a magnetic dipole source from that of an equivalent electric dipole source, and vice versa.

Table A-1. Boundary conditions for Hertz vectors for various dipole sources.

Vertical Magnetic Dipole (VMD)	Magnetic	$M_i\Pi_Z = M_{i+1}\Pi_Z^{i+1}$	$\frac{\partial \Pi_Z^i}{\partial Z} = \frac{\partial \Pi_Z^{i+1}}{\partial Z}$
Vertical Electric Dipole (VED)	Electric	$K_i\Pi_Z^i = K_{i+1}\Pi_Z^{i+1}$	$\frac{\partial \Pi_Z^i}{\partial Z} = \frac{\partial \Pi_Z^{i+1}}{\partial Z}$
Horizontal Magnetic Dipole (HMD)	Magnetic	$k_i^2\Pi_X^i = k_{i+1}^2\Pi_X^{i+1}$ $\nabla\cdot\mathbf{\Pi}^i = \nabla\cdot\mathbf{\Pi}^{i+1}$	$M_i\Pi_Z^i = M_{i+1}\Pi_Z^{i+1}$ $M_i\frac{\partial \Pi_X^i}{\partial Z} = M_{i+1}\frac{\partial \Pi_X^{i+1}}{\partial Z}$
Horizontal Electric Dipole (HED)	Electric	$k_i^2\Pi_X^i = k_{i+1}^2\Pi_X^{i+1}$ $\nabla\cdot\mathbf{\Pi}^i = \nabla\cdot\mathbf{\Pi}^{i+1}$	$K_i\Pi_Z^i = K_{i+1}\Pi_Z^{i+1}$ $K_i\frac{\partial \Pi_X^i}{\partial Z} = K_{i+1}\frac{\partial \Pi^{i+1}}{\partial Z}$

Table A-2(a). Coefficients $a_i(\lambda)$, $b_i(\lambda)$, and $c_i(\lambda)$ for vertical dipole source.

		Two-layer earth	Half-space
Vertical Magnetic Dipole	a_0	$\frac{R_{01}+R_{12}\beta}{1-R_{10}R_{12}\beta}$	R_{01}
	a_1	$\frac{\eta_{01}T_{01}}{1-R_{10}R_{12}\beta}$	$\eta_{01}T_{01}$
	a_2	$\frac{\eta_{01}T_{01}R_{12}\beta}{1-R_{10}R_{12}\beta}$	0
	a_3	$\frac{\eta_{01}T_{01}\eta_{12}T_{12}}{1-R_{10}R_{12}\beta}$	$\eta_{01}T_{01}$
Vertical Electric Dipole	a_0	$\frac{X_{01}+X_{12}\beta}{1-X_{10}X_{12}\beta}$	X_{01}
	a_1	$\frac{\xi_{01}S_{01}}{1-X_{10}X_{12}\beta}$	$\xi_{01}S_{01}$
	a_2	$\frac{\xi_{01}S_{01}X_{12}\beta}{1-X_{10}X_{12}\beta}$	0
	a_3	$\frac{\xi_{01}S_{01}\xi_{12}S_{12}}{1-X_{10}X_{12}\beta}$	$\xi_{01}S_{01}$

The various parameters used in the solutions are listed in Table A-3.

The expressions X_{ij}, S_{ij}, R_{ij}, and T_{ij} are the Fresnel plane-wave reflection and transmission coefficients. The subscript notation ij has the following meaning: subscript i denotes the medium from which the plane wave is incident on the plane boundary between media i and j. For example, the subscripts 01 mean a plane-wave incident from the air on the boundary between the air and the first layer of the earth. The X_{ij} and S_{ij} are the reflection and transmission coefficients respectively for a TM plane wave; the R_{ij} and S_{ij} are the reflection and transmission coefficients for a TE plane wave.

APPENDIX B: PLANE-WAVE SPECTRUM AND EVALUATION OF INTEGRALS

The physical meaning of the integral expressions for the various Hertz vector solutions is much more apparent when the plane-wave spectrum notation is used. The form of the plane-wave spectrum used throughout is obtained by defining three complex angles, $\theta_0, \theta_1, \theta_2$, and transforming the integration variable by setting

$$\lambda = k_0 \sin\theta_0 = k_1 \sin\theta_1 = k_2 \sin\theta_2. \quad \text{(B-1)}$$

The angle θ_0 is used in the region $Z \geq 0$, θ_1 in the region $-d \leq Z \leq 0$, and θ_2 in the region $Z \leq -d$. The above transformation is just an expression of Snell's law. A plane-wave incident from the region $Z > 0$ on the earth's surface at an angle θ_0 to the z-axis is refracted into medium 1 at an angle θ_1, and to the z-axis and into medium 2 at an angle θ_2, as illustrated in Figure B-1. The reader is referred to Clemmow (1966) for details.

The expressions for the Hertz vectors in equations (10) through (18) transform as follows, where the Π_Z^0 for a vertical dipole has been chosen as an example:

$$\Pi_Z^0 = \frac{e^{ik_0R}}{WR} + \frac{ik_0}{2W}\int_c \sin\theta_0 a_0(\theta_0) \cdot e^{ik_0 \cos\theta_0 (Z+h)} H_0^1(k_0\rho \sin\theta_0) d\theta_0. \quad \text{(B-2)}$$

The integration contour C runs from $-\pi/2+i\infty$ to $-\pi/2$ along the real θ_0 axis to $\pi/2$ and then to $\pi/2-i\infty$, as illustrated in Figure B-2. For the angles θ_i, the contour C is obtained from equation (B-1). The P_i transform to $-ik_i \cos\theta_i$, where the negative sign is chosen in order to satisfy the radiation condition. Substituting for P_i in the Fresnel coefficients of Table A-3 results in the more familiar form

$$X_{ij} = \frac{\left(\frac{K_j}{K_i}\right)^{1/2} \cos\theta_i - \left(\frac{M_j}{M_i}\right)^{1/2} \cos\theta_j}{\left(\frac{K_j}{K_i}\right)^{1/2} \cos\theta_i + \left(\frac{M_j}{M_i}\right)^{1/2} \cos\theta_j}, \quad \text{(B-3)}$$

where the TM reflection coefficient is shown as an example.

The integral expressions can be approximately evaluated by manipulating the integration contour C in the complex θ plane. The approach is to replace the Hankel function by its asymptotic expansion, which is valid when the argument is considerably greater than unity.

Table A-2(b). Coefficients $a_i(\lambda)$, $b_i(\lambda)$, and $c_i(\lambda)$ for horizontal dipole sources.

		Two-layer earth	Half-space
HMD	b_0	$\dfrac{X_{01}+X_{12}\beta}{1-X_{10}X_{12}\beta}$	X_{01}
	b_1	$\dfrac{\gamma_{01}S_{01}}{1-X_{10}X_{12}\beta}$	$\gamma_{01}S_{01}$
	b_2	$\dfrac{\gamma_{01}S_{01}X_{12}\beta}{1-X_{10}X_{12}\beta}$	0
	b_3	$\dfrac{\gamma_{01}S_{01}\gamma_{12}S_{12}}{1-X_{10}X_{12}\beta}$	$\gamma_{01}S_{01}$
	c_0	$\dfrac{1}{2P_0}\dfrac{(\gamma_{01}-1)T_{01}(1+R_{12}\beta)S_{01}(1+X_{12}\beta)-(\gamma_{21}-1)\eta_{01}T_{10}T_{12}m_{01}\gamma_{01}S_{01}\gamma_{12}S_{12}\beta}{(1-R_{10}R_{12}\beta)(1-X_{10}X_{12}\beta)}$	$\dfrac{1}{2P_0}(\gamma_{01}-1)T_{01}S_{01}$
	c_1	$\dfrac{1}{2P_0}\dfrac{(\gamma_{01}-1)\eta_{01}T_{01}S_{01}(1+X_{12}\beta)-(\gamma_{21}-1)R_{10}T_{12}m_{01}S_{01}\gamma_{12}S_{12}\beta}{(1-R_{10}R_{12}\beta)(1-X_{10}X_{12}\beta)}$	$\dfrac{1}{2P_0}(\gamma_{01}-1)\eta_{01}T_{01}$
	c_2	$\dfrac{1}{2P_0}\dfrac{(\gamma_{01}-1)\eta_{01}T_{01}R_{12}\beta S_{01}(1+\gamma_{12}\beta)-(\gamma_{21}-1)T_{12}m_{01}\gamma_{01}S_{01}\gamma_{12}S_{12}\beta}{(1-R_{10}R_{12}\beta)(1-X_{10}X_{12}\beta)}$	0
	c_3	$\dfrac{1}{2P_0}\dfrac{(\gamma_{01}-1)\eta_{01}T_{01}\eta_{12}T_{12}S_{01}(1+X_{12}\beta)-(\gamma_{21}-1)\eta_{12}T_{12}(1+R_{10}R_{12}\beta)m_{01}\gamma_{01}S_{01}\gamma_{12}S_{12}}{(1-R_{10}R_{12}\beta)(1-X_{10}X_{12}\beta)}$	$\dfrac{1}{2P_0}(\gamma_{01}-1)\eta_{01}T_{01}$
HED	b_0	$\dfrac{R_{01}+R_{12}\beta}{1-R_{10}R_{12}\beta}$	R_{01}
	b_1	$\dfrac{\gamma_{01}T_{01}}{1-R_{10}R_{12}\beta}$	$\gamma_{01}T_{01}$
	b_2	$\dfrac{\gamma_{01}T_{01}R_{12}\beta}{1-R_{10}R_{12}\beta}$	0
	b_3	$\dfrac{\gamma_{01}T_{01}\gamma_{12}T_{12}}{1-R_{10}R_{12}\beta}$	$\gamma_{01}T_{01}$
	c_0	$\dfrac{1}{2P_0}\dfrac{(\gamma_{01}-1)S_{01}(1+X_{12}\beta)T_{01}(1+R_{12}\beta)-(\gamma_{21}-1)\xi_{10}S_{10}S_{12}m_{01}\gamma_{01}T_{01}\gamma_{12}T_{12}\beta}{(1-R_{10}R_{12}\beta)(1-X_{10}X_{12}\beta)}$	$\dfrac{1}{2P_0}(\gamma_{01}-1)S_{01}T_{01}$
	c_1	$\dfrac{1}{2P_0}\dfrac{(\gamma_{01}-1)\xi_{01}S_{01}T_{01}(1+R_{12}\beta)-(\gamma_{21}-1)S_{12}X_{10}m_{01}\gamma_{01}T_{01}\gamma_{12}T_{12}\beta}{(1-R_{10}R_{12}\beta)(1-X_{10}X_{12}\beta)}$	$\dfrac{1}{2P_0}(\gamma_{01}-1)\xi_{01}S_{01}$
	c_2	$\dfrac{1}{2P_0}\dfrac{(\gamma_{01}-1)\xi_{01}S_{01}X_{12}\beta(1+R_{12}\beta)T_{01}-(\gamma_{21}-1)S_{12}m_{01}\gamma_{01}T_{01}\gamma_{12}T_{12}\beta}{(1-R_{10}R_{12}\beta)(1-X_{10}X_{12}\beta)}$	0
	c_3	$\dfrac{1}{2P_0}\dfrac{(\gamma_{01}-1)\xi_{01}S_{01}\xi_{12}S_{12}T_{01}(1+R_{12}\beta)-(\gamma_{21}-1)\xi_{12}S_{12}(1+\gamma_{01}\beta)m_{01}\gamma_{01}T_{01}\gamma_{12}T_{12}}{(1-R_{10}R_{12}\beta)(1-X_{10}X_{12}\beta)}$	$\dfrac{1}{2P_0}(\gamma_{01}-1)\xi_{01}S_{01}$

Table A-3. Parameters used and Fresnel coefficients.

Parameters	
$\gamma_{ij} = \dfrac{k_i^2}{k_j^2}$	$\xi_{ij} = \dfrac{K_i}{K_j}$
$m_{ij} = \dfrac{P_i}{P_j}$	$\beta = e^{-2P_1 d}$
$\eta_{ij} = \dfrac{M_i}{M_j}$	$k_i^2 = K_i M_i (2\pi)^2$

TM Fresnel Coefficients

Reflection:	$X_{ij} = \dfrac{K_j P_i - K_i P_j}{K_j P_i + K_i P_j}$	
Transmission:	$S_{ij} = \dfrac{2K_j P_i}{K_j P_i + K_i P_j}$	
Relations:	$X_{ij} = -X_{ji}$	$X_{ij} = S_{ij} - 1$
	$X_{ij} = 1 - S_{ji}$	$S_{ij} = \dfrac{\xi_{ji}}{m_{ji}} S_{ji}$

TE Fresnel Coefficients

Reflection:	$R_{ij} = \dfrac{M_j P_i - M_i P_j}{M_j P_i + M_i P_j}$	
Transmission:	$T_{ij} = \dfrac{2M_j P_i}{M_j P_i + M_i P_j}$	
Relations:	$R_{ij} = -R_{ji}$	$R_{ij} = T_{ij} - 1$
	$R_{ij} = 1 - T_{ji}$	$T_{ij} = \dfrac{\eta_{ji}}{m_{ji}} T_{ji}$

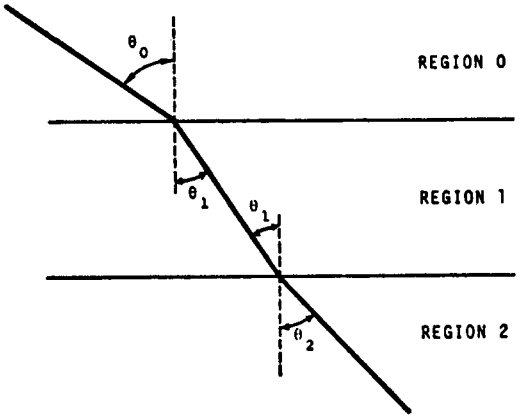

FIG. B-1. Illustration of integration variables θ_0, θ_1, and θ_2 and Snell's law.

$$H_0^1(t) = e^{i(t-(\pi/4))}\left(\frac{2}{\pi t}\right)^{1/2} \cdot \left(1 + \frac{1}{i8t} + \cdots\right), \tag{B-4}$$

and

$$H_1^1(t) = e^{i(t-(3\pi/4))}\left(\frac{2}{\pi t}\right)^{1/2} \cdot \left(1 - \frac{3}{i8t} + \cdots\right). \tag{B-5}$$

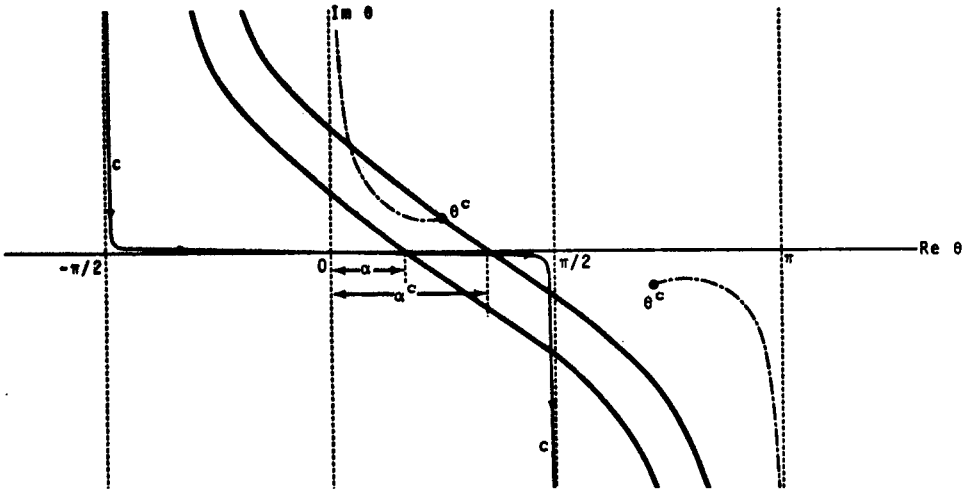

FIG. B-2. Complex θ-plane showing contour C, saddle-point contours Γ and Γ', and the positions of the branch point θ^c and branch cut (chain line).

Substitution into the integrals, such as that in equation (B-2), results in an expression of the form

$$e^{iZk\cos\theta+ik\rho\sin\theta} \tag{B-6}$$

in the integrand, which can be written as

$$e^{ikR\cos(\theta-\alpha)}, \tag{B-7}$$

where $R=(\rho^2+Z^2)^{1/2}$, and R and α are just the length and direction of the geometric-optics ray-path. An integral with exponential of the form (B-7) is amenable to the saddle-point method integration, where $\theta=\alpha$ is the saddle point. By deforming C to the contour of most rapid descent away from the saddle point Γ one obtains an asymptotic series in the parameter $(kR)^{-1}$ for the integral. The leading term in the series is the geometric-optics solution to the problem.

The saddle-point contour Γ is defined from the argument of the exponential in expression (B-7). Along the contour Γ,

$$ikR\cos(\theta-\alpha) = ikR - kRs^2, \tag{B-8}$$

where

$$s^2 = -\sin(\theta'-\alpha)\sinh\theta'', \tag{B-9}$$

and

$$\theta = \theta' + i\theta''. \tag{B-10}$$

The contour Γ is then given by the equation

$$\cos(\theta'-\alpha)\sinh\theta'' = 1 \tag{B-11}$$

and is illustrated in Figure B-2.

An excellent evaluation of the particular types of integrals that appear in the text is given by Brekhovskikh (1960), and the reader is referred to this reference for more detailed discussion. In the rest of the discussion, solutions to the integrals valid to the second order in kR^{-1} are used. This involves using the second-order terms in the Hankel-function expansion and then taking the asymptotic solution to the integrals to the second order. The integrals in the text have two forms:

$$I_1 = \frac{ik}{2W}\int_c \sin\theta A(\theta) \cdot e^{ikZ\cos\theta}H_0^1(k\rho\sin\theta)d\theta, \tag{B-12}$$

and

$$I_2 = \frac{ik^2}{2W}\int_c \sin^2\theta A(\theta) \cdot e^{ikZ\cos\theta}H_1^1(k\rho\sin\theta)d\theta. \tag{B-13}$$

The solutions to the second order are given by

$$I_1 \simeq \frac{e^{ikR}}{WR}\left\{A(\alpha) - \frac{i}{2kR}\cdot\left[A''(\alpha)+A'(\alpha)\cot\alpha\right]\right\}, \tag{B-14}$$

and

$$I_2 \simeq -ik\sin\alpha\frac{e^{ikR}}{WR}\left\{A(\alpha)-\frac{i}{2kR}\cdot\left[A''(\alpha)+3\cot\alpha A'(\alpha)-2A(\alpha)\right]\right\}. \tag{B-15}$$

Solutions (B-14) and (B-15) are valid as long as $A(\theta)$ is a slowly varying function of θ near the saddle point α. This assumption is valid provided $A(\theta)$ does not have a singular point near α. In the expressions for the various $A(\theta)$ appearing in the text, branch points and poles of $A(\theta)$ are of the utmost importance in the solutions. The branch points of $A(\theta)$ are the critical angles of the boundaries in the problem. The critical angles enter all the $A(\theta)$ through the relation

$$\cos\theta_j = \pm\left[1-\gamma_{ij}\sin^2\theta_i\right]^{1/2} \tag{B-16}$$

in all the Fresnel coefficients subscripted ij.

The radical splits the complex θ-plane into two Riemann sheets with branch points at

$$\sin\theta_{ij}^c = \pm\frac{k_j}{k_i}. \tag{B-17}$$

For the two-layer earth there are two boundaries which give two critical angles and result in a four-sheeted θ-plane. In the half-space earth problem, the complex θ-plane is two-sheeted. The convention followed throughout is that of taking the positive square root. The surface defined in this manner is referred to as the upper Riemann surface. For one to evaluate the integrals, the branch cuts from the branch points must be defined. The convention used here is the same as that of Ott and Brekhovskikh, who define the branch lines as those contours along which the imaginary part of

equation (B-16) is zero. The branch line is the chain line in Figure B-2.

The branch points must be taken into account for saddle-point angles greater than α^c. As illustrated in Figure B-2, for $\alpha > \alpha^c$, in order to deform contour C into Γ, the branch point θ^c must be crossed. A modified integration contour to take θ^c into account is shown in Figure B-3. As long as α and θ^c are well separated, the saddle-point and branch-point contributions can be evaluated separately. The contribution of the branch point is a second-order effect (Ott, 1941) as long as $\alpha \neq \theta^c$ and an approximate evaluation of the branch-point contribution can be obtained using the method of steepest descent. In general, α^c is obtained by substituting $\theta = \theta^c$ in equation (B-11). In the particular case of two perfect dielectric materials, i and j, forming the boundary,

$$\overset{c}{\alpha}_{ij} = \sin^{-1}\left(\frac{k_i}{k_j}\right), \qquad k_i < k_j, \quad \text{(B-18)}$$

and

$$\overset{c}{\alpha}_{ij} = \sin^{-1}\left(\frac{k_j}{k_i}\right), \qquad k_j < k_i. \quad \text{(B-19)}$$

The steepest-descent evaluation of the branch-point contribution is summarized as follows: The branch cut integral has the form

$$I_B = \frac{ik_i^{(n+1)}}{2W} \int_B \sin^{n+1}\theta_i A(\theta_i) \cdot e^{ik_i Z \cos\theta_i} H_n^1(k_i\rho \sin\theta_i) d\theta_i, \quad \text{(B-20)}$$

where the contour B runs from $i\infty$ to θ^c on the left of the branch cut and from θ^c back to $i\infty$ along the right of the branch cut. For approximate evaluation, I_B is rewritten

$$I_B \simeq -\frac{ik_i^{n+1}}{2W} e^{-i(2n+1)\pi/4}\left(\frac{2}{\pi k_i\rho}\right)^{1/2} \cdot \int_{B'} \sin^{n+(1/2)}\theta_i [A^+(\theta_i) - A^-(\theta_i)] \cdot e^{ik_i R\cos(\theta_i - \alpha)} d\theta_i, \quad \text{(B-21)}$$

where the Hankel function has been replaced by the first term of its asymptotic expansion. The superscripts + and − on $A(\theta_i)$ denote the sign of the radical in equation (B-16) taken in $A(\theta_i)$, and the contour B' runs from θ_{ij}^c to $i\infty$. The contour B' is deformed into the steepest-descent contour, B'', away from θ_{ij}^c. The path of steepest descent is defined by

$$\text{Im } ik_i R\cos(\theta_i - \alpha) = \text{constant} \quad \text{(B-22)}$$

and is illustrated by the dotted line in Figure B-3. On the assumption that $k_i R \gg 1$, so that only

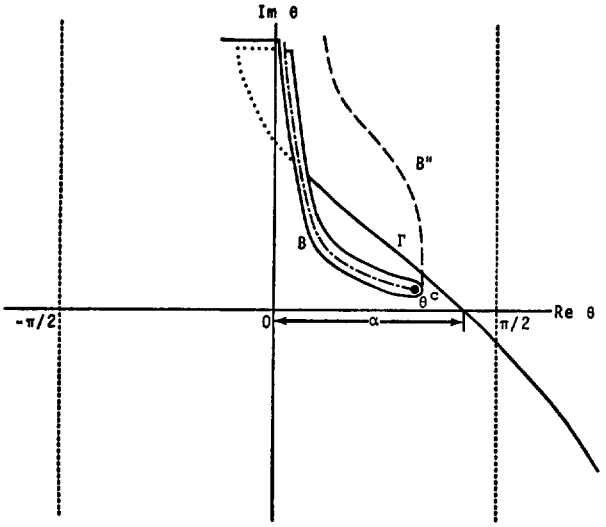

FIG. B-3. Complex θ-plane showing modification of saddle-point contour Γ to contour B in order to account for branch-point contribution, and path of steepest descent (dotted line).

angles very close to θ_{ij}^c contribute significantly to the integral, θ_i can be set equal to θ_{ij}^c in all expressions in the integrand except for the radical. In general,

$$A^+(\theta_i) - A^-(\theta_i) = F(\theta_i)\cos\theta_j, \quad \text{(B-23)}$$

and the integral is approximately

$$I_B = \frac{-ik_i^{n+1}}{2W} e^{-i(2n+1)\pi/4} \cdot \left(\frac{2}{\pi k_i \rho}\right)^{1/2} \sin^{n+(1/2)} \theta_{ij}^c F(\theta_{ij}^c) \quad \text{(B-24)}$$
$$\cdot \int_{B'} \cos\theta_j e^{ik_i R\cos(\theta_i-\alpha)} d\theta_i.$$

For low-loss media, θ_{ij}^c is close to the real axis for $k_j<k_i$ or close to the $\pi/2$ line for $k_i<k_j$ in the complex θ_i plane. The method of solution of the integral in equation (B-24) is slightly different in the two situations, but the results are identical. Here, the θ_{ij}^c will be assumed close to the real axis. The approximate solution is valid for θ_{ij}^c near the $\pi/2$ line.

Along the steepest-descent contour near θ_{ij}^c,

$$\theta_i \approx \theta_{ij}^c + iu, \quad \text{(B-25)}$$

where u is much less than unity. Then,

$$\cos\theta_j \simeq -e^{-i\pi/4}\sqrt{2u}\left(\frac{k_i^2 - k_j^2}{k_j^2}\right)^{1/4}, \quad \text{(B-26)}$$

and

$$ik_iR\cos(\theta_i-\alpha) \simeq ik_iR\cos(\theta_{ij}^c-\alpha) - k_iR\sin(\alpha-\theta_{ij}^c)u. \quad \text{(B-27)}$$

The integral in equation (B-24) becomes

$$-ie^{-i\pi/4}\sqrt{2}\left(\frac{k_i^2 - k_j^2}{k_j^2}\right)^{1/4} e^{ik_iR\cos(\theta_{ij}^c-\alpha)} \cdot \int_{B''} \sqrt{u}\, e^{-k_iR\sin(\alpha-\theta_{ij}^c)u} du. \quad \text{(B-28)}$$

Now, the integral

$$\int_{B''} \sqrt{u}\, e^{-\delta u} du \simeq \int_0^\infty x^2 e^{-\delta x^2} dx = \frac{1}{2}\sqrt{\frac{\pi}{\delta^3}}. \quad \text{(B-29)}$$

Rearranging equations (B-24) and (B-28), one finally obtains

$$I_B = \frac{ik_j^n}{2W\rho^2} \frac{e^{-in(\pi/2)} F(\theta_{ij}^c)}{(k_i^2 - k_j^2)^{1/2}} \cdot (1 - \cot\alpha\tan\theta_{ij}^c)^{-3/2} \cdot e^{ik_j\rho\sin\theta_{ij}^c + ik_i\cos\theta_{ij}^c Z}, \quad \text{(B-30)}$$

which must be added to equations (B-14) and (B-15) when $\alpha>\alpha^c$.

The assumption in the saddle-point and steepest-descent techniques that $kR\gg1$ is reasonably valid when R is greater than two wavelengths, since $k>2\pi$ and $kR>10$ when $R>2$.

The poles of the integrands are also of importance in the solutions. Discussion of their role in the solutions is given in the text.

ACKNOWLEDGMENTS

The author is grateful to the National Research Council of Canada for a fellowship which supported this work.

This work is the first paper in a series providing the background for the Surface Electrical Properties Experiment planned for the Apollo 17 lunar mission.

REFERENCES

Brekhovskikh, L. M., 1960, Waves in layered media: New York, Academic Press.

Budden, K. G., 1961, The wave-guide mode theory of wave propagation: Englewood Cliffs, Prentice-Hall, Inc.

Clemmow, P. C., 1966, The plane wave spectrum representation of electromagnetic fields: New York, Pergamon Press.

El-Said, M. A. H., 1956, Geophysical prospection of underground water in the desert by means of electromagnetic interference fringes: Proc. I.R.E., v. 44, p. 24–30 and 940.

Evans, S., 1963, Radio techniques for the measurement of ice thickness: The Polar Record, v. 11, p. 406–410 and 795.

Katsube, T. J., and Collett, L. S., 1971, Electrical properties of Apollo 11 and 12 lunar samples, *in* Proceedings of the Second Lunar Science Conference, Houston, Texas, edited by A. A. Levinson: Cambridge, Mass. Inst. Tech. (in press).

Norton, K. A., 1937, The propagation of radio waves over the surface of the earth and in the upper atmo-

sphere, Part I: Proc. I.R.E., v. 24, p. 1367–1387; Part II: Proc. I.R.E., v. 25, p. 1203–1236.
Ott, H., 1941, Reflexion und Brechung von Kugelwellen; Effekle Q. Ordnung: Ann. Physik, v. 41, p. 443–466.
——— 1943, Die Sattelpunktsmethode in der Umgeburg eines Pols mit Anwendungen auf die Wellenoptik und Akustic: Ann. Physik, v. 43, p. 393.
Rossiter, J. R., LaTorraca, G. A., Annan, A. P. Strangway, D. W., and Simmons, G., 1973, Radio interferometry depth sounding: part II—experimental results: Geophysics, this issue.
Saint-Amant, M., and Strangway, David W., 1970, Dielectric properties of dry, geologic materials: Geophysics, v. 35, p. 624–645.
Sommerfeld, A., 1909, Uber die Ausbreitung der Wellen in der Drahtlosen telegraphie: Ann. Physik, v. 28, p. 665–737.
——— 1949, Partial differential equations in physics: New York, Academic Press.
Strangway, D. W., 1969, Moon: Electrical properties of the uppermost layers: Science, v. 165, p. 1012–1013.
Van der Waerden, B. L., 1951, On the method of saddle points: Appl. Sci. Res., B2, p. 33–45.
Wait, J. R., 1951, The magnetic dipole over the horizontally stratified earth: Can. J. Phys., v. 29, p. 577–592.
Wait, J. R., 1970, Electromagnetic waves in stratified media, 2nd edition: New York, The Macmillan Co.
Ward, S. H., and Dey, A., 1971, Lunar surface electromagnetic sounding: A theoretical analysis, I.E.E.E. Trans. GE-9, no. 1, p. 63–71.